## Sakarya Üniversitesi Fen Bilimleri Dergisi Sakarya University Journal of Science



e-ISSN: 2147-835X Publisher: Sakarya University

Vol. 29, No. 2, 160-170, 2025 DOI: https://doi.org/10.16984/saufenbilder.1590407

Research Article

## Structural Properties and Bandgap Energy of Ga-doped Garnet-type Li<sub>7</sub>La<sub>3</sub>Zr<sub>2</sub>O<sub>12</sub> (LLZO) **Solid Electrolyte Depending on Sintering Atmosphere**



Selçuk University, Faculty of Science, Department of Physics, Konya, Türkiye, sevdaaktas@selcuk.edu.tr, ror.org/045hgzm75

#### ARTICLE INFO

#### ABSTRACT

Keywords: Garnet-type LLZO solid electrolyte Sintering atmosphere DRS Band gap energy



Article History: Received: 24.11.2024 Revised: 07.02.2025 Accepted: 05.03.2025

Online Available: 15.04.2025

Developing solid-state batteries for higher energy densities and safety has been a popular research subject in recent years. Since their first report, Li<sub>7</sub>La<sub>3</sub>Zr<sub>2</sub>O<sub>12</sub>(LLZO) solid electrolytes have attracted extended attention due to their high ionic conductivity, chemical stability, and wide electrochemical window. Although LLZO fulfills all the requirements for high energy density and a longer lifespan, its intrinsic electronic conductivity accelerates the Li dendrite growth short-circuiting the battery. In this study, we have applied air and oxygen sintering atmospheres to prepare two types of Ga-doped LLZO pellets, to identify the effect of sintering atmospheres on the physical properties such as crystal phase, ionic conductivity, roughness, and electronic band gap energy (Eg). Both the crystal structures were found to be in cubic phase with a relatively small amount of secondary phase impurities. On the other hand, the oxygen-sintered sample showed better properties with high ionic conductivity of 1.04x10<sup>-4</sup> Scm<sup>-1</sup>, lower surface root-mean-square roughness of 0.1833 μm, and a relative density of 90.5%. Furthermore, the electronic indirect band gap energy of the oxygen-sintered sample was larger, E<sub>g</sub>=5.77 eV, which is desired for lower electrical conductivity. It is important to note that the precise determination of Eg values of powders would be erroneous through Ultraviolet-Visible (UV-Vis) absorption spectroscopy due to the scattering effects of solids. So, to the best of our knowledge, for the first time, this study reports E<sub>g</sub> values of oxygen and air-sintered LLZO determined by the Kubelka-Munk model on Ultraviolet-Visible-Near Infra-Red (UV-Vis-NIR) diffuse reflectance spectroscopy.

#### 1. Introduction

Garnet-type Li<sub>7</sub>La<sub>3</sub>Zr<sub>2</sub>O<sub>12</sub> (LLZO) solid electrolytes can be replaced with organic flammable non-safe liquid electrolytes due to their advantages, such as high ionic conductivity, wide electrochemical window, and compatibility with high-voltage cathodes and Li metal anodes. benefits make garnet-type electrolytes increasingly recognized as a good candidate for solid-state batteries compared to other solid electrolytes such as sulfides, halides, NaSICONs, and polymers [1-8]. However, when Li metal is used as the anode, lithium dendrites grow through LLZO and lead to a battery shortcircuit which is challenging to prevent [9-10].

Although recent studies have indicated the factors contributing to dendrite formation, such as the low relative density of LLZO, preexisting cracks on the surface, and poor contact between LLZO and Li metal, this issue has not been solved [11-13]. On the other hand, Han et al. reported that the electronic conductivity of LLZO is mostly responsible for Li dendrite formation [14]. Although the solid electrolyte and the alloy interphase at the Li/Solid electrolyte interface have low electronic conductivities, the enlarged 'effective' contact area between Li and the solid electrolyte could lower the potential in the solid electrolyte, accelerating Li dendrite formation [14]. This means that at even very low electronic conductivities Li dendrites can grow. In recent

Cite as: S. Saran (2025). Structural Properties and Bandgap Energy of Ga-doped Garnet-type Li7La3Zr2O12 (LLZO) Solid Electrolyte Depending on Sintering Atmosphere, Sakarya University Journal of Science, 29(2), 160-170. https://doi.org/10.16984/saufenbilder.1590407



reports, to suppress the growth of Li dendrites, electronic insulator layers have been deposited on the LLZO surface, and some compounds have been introduced into LLZO to contract electron-blocking properties, especially at the grain boundaries [15-16].

On the other hand, most current research on LLZO is focused on improving the ionic conductivity with single-element and dual-element doping strategies. However, while these strategies increase the ionic conductivity, they may also increase the electronic conductivity. That's why it is important to consider a lower electronic conductivity while considering a high ionic conductivity. In that manner, UV-Vis diffuse reflectance spectroscopy (DRS) might be a convenient and easy way to determine the electronic band gap of newly synthesized solid electrolytes with high ionic conductivity.

The electronic band gap (E<sub>g</sub>) that can be analyzed experimentally with Ultraviolet-Visible (UV-Vis) spectroscopy is an important feature of materials that determines their electronic conductivity. literature, In the theoretical indirect band gap of LLZO is given as 5.918 eV [17]. Experimentally, there are a few studies on the electronic band gap of LLZO. In one of the reports, a polished transparent LLZO which is complicated to prepare was studied with UV-Vis absorption spectroscopy. In that study, the indirect electronic band gap was determined as 5.46 eV for Al-doped LLZO [18]. Another study reported a band gap of ~ 6 eV determined via the UV-Vis absorption spectroscopy of LLZO powders [19].

Although UV-Vis absorption spectroscopy is frequently used to analyze the band gap of solutions or thin films, it is an inadequate technique to determine the band gap value of powder samples. Because in the case of powders, the estimated wavelength of absorbed photons is erroneous due to the scattering effects [20-21]. On the other hand, the dispersion of LLZO in most liquids is not stable [22]. Consequently, the LLZO powder concentration in the liquid changes in time which is an obstacle to estimating the accurate E<sub>g</sub> with the UV-Vis absorption spectroscopy.

DRS is a widely used technique to analyze the optical properties of powder samples [23-24]. To the best of our knowledge, the powder LLZO solid electrolyte has not been characterized via diffuse reflectance spectroscopy. The electronic band gap of materials like other physical and chemical properties can be affected by the synthesis conditions and methods, we therefore synthesized Ga-doped LLZO solid electrolytes in oxygen (O<sub>2</sub>) and air atmospheres [25]. Then, crystal structures, morphologies, relative densities. electronic bandgaps, and conductivities of the samples were characterized.

#### 2. General Methods

Li<sub>6.4</sub>Ga<sub>0.2</sub>La<sub>3</sub>Zr<sub>2</sub>O<sub>12</sub> solid electrolytes were synthesized with a solid-state reaction method by using the precursor powders (purity: 99.9%) of Li<sub>2</sub>CO<sub>3</sub>, Ga<sub>2</sub>O<sub>3</sub>, La<sub>2</sub>O<sub>3</sub>, and ZrO<sub>2</sub> in the desired stoichiometric ratio according to the following chemical equation [26],

$$3.2Li_2CO_3 + 0.1Ga_2O_3 + 1.5La_2O_3 + 2ZrO_2$$
  
 $\rightarrow Li_{6.4}Ga_{0.2}La_3Zr_2O_{12} + 3.2CO_2$  (1)

The powder mixture was then subjected to a series of ball milling and heat treatments. First, the mixture was ball milled in isopropanol at 400 rpm with 6-minute reversal intervals for 5 hours using a Retsch PM100 ball grinder. The powders were then dried to remove the isopropanol. Next, the dried powders were heated at 900 °C for 8 hours in air and O<sub>2</sub> atmospheres. In the second step, the ball milling was repeated at 350 rpm in a dry system. Finally, the powders were pressed into pellets with a diameter of 13 mm and a thickness of 1 mm. Before sintering at 1230 °C for 2 hours in air and O<sub>2</sub>, the pellets were buried in the mother powder to compensate for Li loss at high temperatures. Before characterization, pellets were polished to remove the mother powder and have a smooth surface.

Crystal structure analysis was conducted using a Bruker D8 X-ray diffractometer (XRD) with a CuK $\alpha$  source. Electrochemical impedance spectroscopy (EIS) of the samples with silver-coated electrodes was measured between two cylindrical stainless steel at room temperature in the frequency range of 1-10<sup>5</sup> Hz with an AC

signal of 10 mV by Gamry PCI4/750 Potentiostat.

While a ZEISS LS 10 model scanning electron microscopy (SEM) was used to image the micron-sized area of the pellet's surface, a Filmetrics Profilm 3D model optical profilometer was used to image the millimeter-sized area (2 mm x 2 mm) of the pellet's surface.

The theoretical and experimental densities of the pellets were calculated using the lattice parameters obtained from XRD data refinement and the Archimedes principle, respectively. Bruker, VERTEX70 model spectrometer was used to collect Fourier transform infrared (FTIR) data between wavenumber of 4000-400 cm<sup>-1</sup> in air. Finally, to study the electronic band gap energy of powder samples with a thickness of 1 mm, the Ultraviolet-Visible Near-Infra-Red (UV-Vis-NIR) diffuse reflection spectrum was collected between 200-1400 nm wavelengths with Shimadzu, ISR-603 spectrometer and the Ultraviolet-Visible (UV-Vis) absorption spectrum was collected between 200-1400 nm wavelengths with Jasco, V-670 spectrometer.

#### 3. Results and Discussion

XRD data in Fig. 1 shows that the atmosphere does not play a crucial role in the crystal structures, since all the samples heated in air and O<sub>2</sub> have the same diffraction peaks. When the samples are sintered at 1230 °C, diffraction peaks become sharper, indicating a well-crystallized cubic phase (2241539-CIF) [27]. The XRD data were analyzed with MAUD software [28]. According to the Rietveld refinement shown in Table 1, Li<sub>6.4</sub>Ga<sub>0.2</sub>La<sub>3</sub>Zr<sub>2</sub>O<sub>12</sub> formed with a space group of I-43d and a lattice parameter of 12.98Å. Moreover, these samples show a relatively small amount of secondary phases La<sub>2</sub>Zr<sub>2</sub>O<sub>7</sub> and La<sub>2</sub>O<sub>3</sub>. These secondary phases are common impurity phases in literature and usually form at high temperatures [29].

SEM micrographs of the pellet surfaces after the final sintering step at 1230 °C in O<sub>2</sub> and air are illustrated in Fig. 2. As seen from the images, the pellet-O<sub>2</sub> has a denser structure, which is similar to that reported in the literature [30]. In other

words, larger pores, where Li dendrites can easily grow, are observed between grains for the pelletair. During the sintering process, oxygen occupies the pores and helps densification by diffusion into the LLZO lattice at high temperatures. On the other hand, trapped air within the pores induces structures with lower density [31].

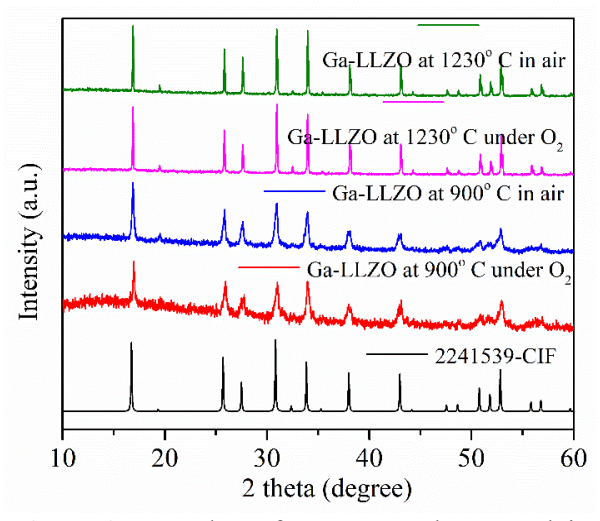


**Figure 1.** XRD data of LLZO samples pre-calcined at 900 °C and finally sintered at 1230 °C in air and O<sub>2</sub> atmospheres

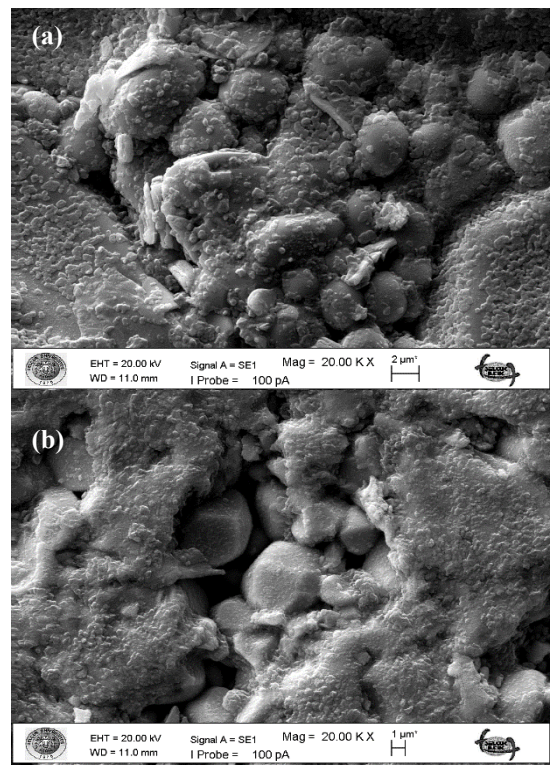


**Figure 2.** SEM micrographs of the surface of Gadoped LLZO pellet sintered at 1230 °C in a) O<sub>2</sub> and b) air atmospheres

**Table 1.** Crystal structure analysis of the samples sintered in air and O<sub>2</sub> at 1230 °C

Sintering Atm.	Phase composition	α	β	γ	a (Å)	c (Å)	Geometry	SG	%(Weight)
	$Li_{6.4}Ga_{0.2}La_3Zr_2O_{12}$	90	90	90	12.98	-	Cubic	I-43d	98.64
Air	$La_2Zr_2O_7$	90	90	90	10.81	-	Cubic	Fd-3m:2	0.13
	La <sub>2</sub> O <sub>3</sub>	90	90	120	3.94	6.13	Hexagonal	P63/mmc	1.23
	$Li_{6.4}Ga_{0.2}La_3Zr_2O_{12}$	90	90	90	12.98	-	Cubic	I-43d	99.14
$O_2$	$La_2Zr_2O_7$	90	90	90	11.04	-	Cubic	Fd-3m:2	0.37
	La <sub>2</sub> O <sub>3</sub>	90	90	120	3.94	6.13	Hexagonal	P63/mmc	0.49

**Table 2.** The total ionic conductivity and density values of Li<sub>6.4</sub>Ga<sub>0.2</sub>La<sub>3</sub>Zr<sub>2</sub>O<sub>12</sub> pellets sintered in air and O<sub>2</sub> at 1230 °C

Sintering Atm.	σ <sub>total</sub> (S cm <sup>-1</sup> )	Apparent Density (g/cm³)	Theoretical Density (g/cm³)	Relative Density (%)
$O_2$	$1.04 \times 10^{-4}$	4.6677	5.156	90.529
Air	5.17x10 <sup>-5</sup>	4.4638	5.150	86.675

SEM results are also confirmed by measuring the apparent density of the pellets using the Archimedes principle. In Table 2, the results are given in terms of relative density calculated through the relation,  $\frac{\rho}{\rho_t}x100$  where  $\rho$  is the measured density and  $\rho_t$  is the theoretical density determined using the lattice parameter obtained by XRD data via the equation,  $\rho_t = ZM/Na^3$  where Z is the number of atoms per unit cell (8), M is the molecular mass, N is Avogadro's number and a is the unit cell parameter [32-33]. The relative density is higher for pellet-O<sub>2</sub> (90.5%) than pellet-air (86.7%) showing well-matched results with the SEM observations.

The increased density of the pellet due to the O<sub>2</sub> sintering atmosphere could be further confirmed with a 3D optical profilometer which creates a 3D surface image for measuring surface profiles and roughness. Fig. 3 shows the topography images taken over an area of 2 mm x 2 mm of the pellets with an optical profilometer. Before optical imaging, the surfaces of the pellets were polished with a 1200-grit number polishing paper. Although polishing conditions were the same, the pellet-O2 showed a shiner surface than pellet-air which reflect can also information about porosity. The topography plot of the pellet-O<sub>2</sub> shows cracks which are most probably due to over-sintering time in O<sub>2</sub>, which we can conclude that the pellets can have a denser structure in a shorter time in the O2 atmosphere compared to air [30]. Although

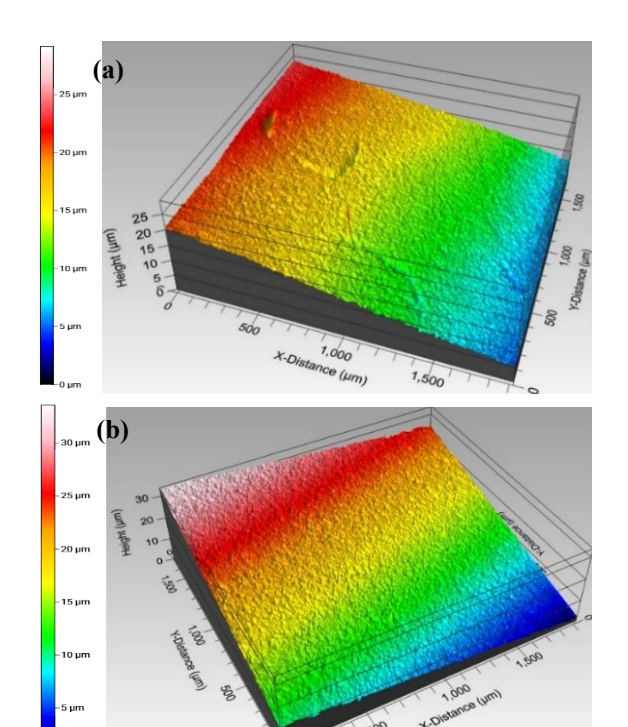


**Figure 3.** Topography plots of Ga-LLZO pellet-O<sub>2</sub> and b) Ga-LLZO pellet-air

pellet- $O_2$  shows cracks on its surface, it still has a lower root-mean-square (RMS) roughness of Rq= 0.1833  $\mu$ m compared to the pellet-air (Rq= 0.4035  $\mu$ m). The higher roughness of the pellet-air could be related to the higher porosity. A lower surface roughness is desired for a solid electrolyte since it helps to create an intimate interface with the Li anode. On the other hand, if there is limited physical contact between the solid electrolyte and the Li anode, the local electric fields arise leading to the acceleration of Li dendrite growth.

Although 3D optical profilometer, a facile and low-priced technique, is not widely used for LLZO surface roughness measurement, it gives comparable results obtained with an atomic force microscope (AFM) in the literature [34-36].

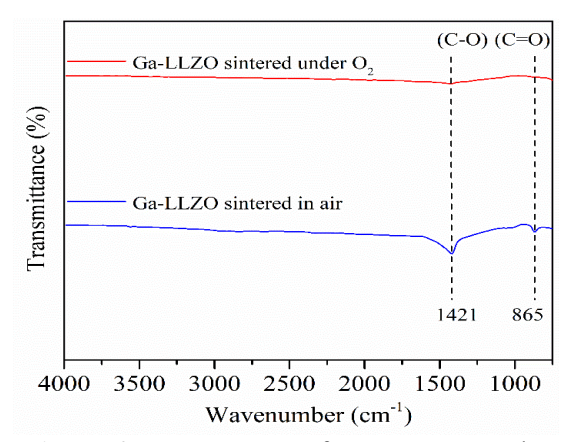


**Figure 4.** FTIR spectra of Ga-LLZO powder sintered in air and O<sub>2</sub>

Before measuring the FTIR spectra in Fig. 4, pellets were polished in air, then milled in a mortar, and immediately stored in a vacuum bag, so the exposure time to air was minimized. The peaks observed at 1421 cm<sup>-1</sup> and 865 cm<sup>-1</sup> are attributed to the impurity of Li<sub>2</sub>CO<sub>3</sub> forms when LLZO is exposed to air [37-39]. Li<sub>2</sub>CO<sub>3</sub> is an undesired impurity since it makes LLZO surface lithiophobic where a limited physical contact at the solid electrolyte-Li anode interface is induced [40]. Although all conditions were the same, these peaks are absent for LLZO sintered in O<sub>2</sub>, indicating that LLZO sintered in O<sub>2</sub> can be more resistive to the formation of Li<sub>2</sub>CO<sub>3</sub> or it is impossible to remove Li<sub>2</sub>CO<sub>3</sub> formed during air sintering from grain boundaries of LLZO. Since the poor contact at the solid electrolyte-Li anode interface accelerates the Li dendrite growth, we can conclude from the FTIR results that the life span of a battery could be longer with an LLZO pellet-O<sub>2</sub>.

Nyquist plots of the EIS spectra of the LLZO pellets on both side silver electrodes and the equivalent circuit used to fit the experimental data are given in Fig. 5. The equivalent circuit is composed of resistors (R) and constant phase elements (CPE) which refers to a non-ideal capacitor [41]. The impedance of CPE is described as  $Z_{CPE} = 1/Q(jw)^n$ , here  $j = \sqrt{-1}$ , w is the frequency, Q is a numerical value with dimension  $Ss^n$  and n is a constant between 0 and

1. The abbreviations b, gb, and el refer to the bulk (interior of the grains), grain boundary (interface of the grains), and electrode (interface of silver electrode and pellet), respectively.

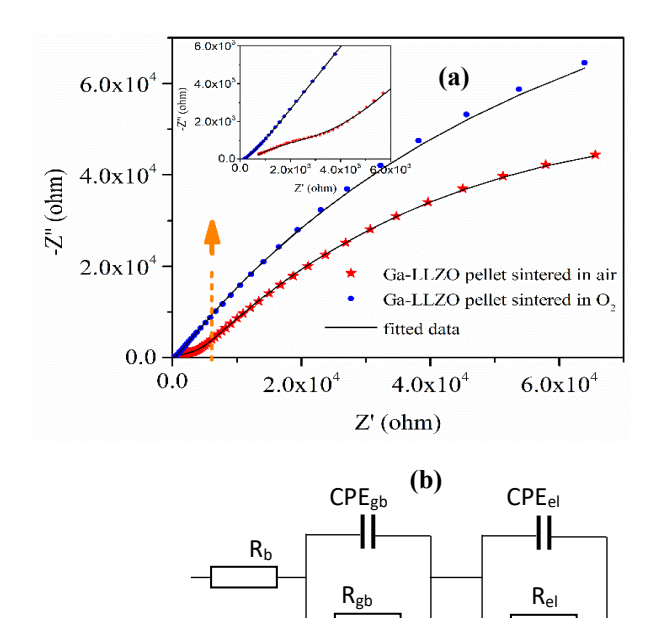


Figure 5. Nyquist plots of EIS measured at room temperature and fitted data of a) Ga-LLZO pellet-O<sub>2</sub> and Ga-LLZO pellet-air, and b) schematic representation of the equivalent circuit that fits experimental data

According to fit results summarized in Table 3, the Li<sub>6.4</sub>Ga<sub>0.2</sub>La<sub>3</sub>Zr<sub>2</sub>O<sub>12</sub> pellet sintered in O<sub>2</sub> shows lower bulk (R<sub>b</sub>) and grain boundary resistances (Rgb) compared to the pellet sintered in air. The ionic conductivities of the pellets were calculated with the equation,  $\sigma = \left(\frac{1}{R}\right)\left(\frac{l}{\sigma}\right)$ R is the total resistivity (bulk and grain boundary), l is the thickness of the pellet and a is the area of the electrode [42]. The oxygensintered pellet shows a higher ionic conductivity of 1.04x10<sup>-4</sup> Scm<sup>-1</sup>, almost two times more than that of the air sintered pellet (Table 2). Since all the conditions except the sintering atmosphere are the same for both samples, the low relative density (high porosity) is probably the main reason for lower ionic conductivity.

High density and high ionic conductivity alone may not be sufficient to suppress the growth of Li dendrites. In addition to high ionic conductivity, a good solid electrolyte should also have low electronic conductivity. As far as we know, the electronic band gap of LLZO depending on synthesis conditions has not been

studied with diffuse reflectance spectroscopy. In Fig. 6, the UV-Vis-NIR diffuse reflectance spectrum of oxygen and air-sintered powders is illustrated. As we mentioned earlier, in the case of powders, UV-Vis diffuse reflectance

spectroscopy is a more convenient technique to determine the electronic band gap since UV-Vis absorption spectroscopy does not consider the scattering effects.

**Table 3.** Fitting results of the analysis of the impedance data of Li<sub>6.4</sub>Ga<sub>0.2</sub>La<sub>3</sub>Zr<sub>2</sub>O<sub>12</sub> pellets sintered in air and O<sub>2</sub> at 1230 °C using the equivalent circuit in Fig. 5 (b),  $\chi^2$  is the square of the standard deviation

Sintering Atmosphere	$R_b(\Omega)$	$ m R_{gb}\left(\Omega ight)$	$Q_{gb}(Ss^n)$	$n_{\mathrm{gb}}$	$\chi^2$
$O_2$	123.3	$1.79 \times 10^3$	8.14x10 <sup>-5</sup>	$3.53 \times 10^{-1}$	1.37x10 <sup>-4</sup>
Air	386.2	$3.46 \times 10^3$	$4.15 \times 10^{-6}$	$4.26 \times 10^{-1}$	$3.14 \times 10^{-4}$

However, DRS may be limited for the samples containing mixed powders for systematic underestimation of the E<sub>g</sub> values. Fortunately, an automated method has been developed to get accurate E<sub>g</sub> values for mixed powders. In the automated method, several concerns have been taken into account as reported in the literature [20]. On the other hand, the thickness of the important for sample is very determination of Eg values. The thickness of the sample should not cause a significant change in its reflectance. That's why for accurate determination of the Eg values, a thickness of more than 0.5 mm must be used to avoid any light transmission [43].

The diffuse reflectance spectroscopy is analyzed with the Kubelka-Munk model,

$$[F(R_{\infty})hv]^{\gamma} = B(hv - E_g) \tag{2}$$

where  $F(R_{\infty})$  is the Kubelka-Munk function, hv is the incident photon energy,  $E_g$  is the electronic band gap, B is a constant, and  $\gamma$  is related to the nature of the band transition, e.g.,  $\gamma = 1/2$ ,  $\gamma = 2$ , for direct and indirect band transitions, respectively [21, 44]. The Kubelka-

Munk function is expressed with the equation (3),

$$F(R_{\infty}) = \frac{K}{S} = \frac{(1 - R_{\infty})^2}{2R_{\infty}}$$
 (3)

where  $R_{\infty}$  is the diffuse reflectance of an optically thick sample, K and S are absorption

and scattering coefficients, respectively [24].  $E_g$  values of the samples can easily be determined

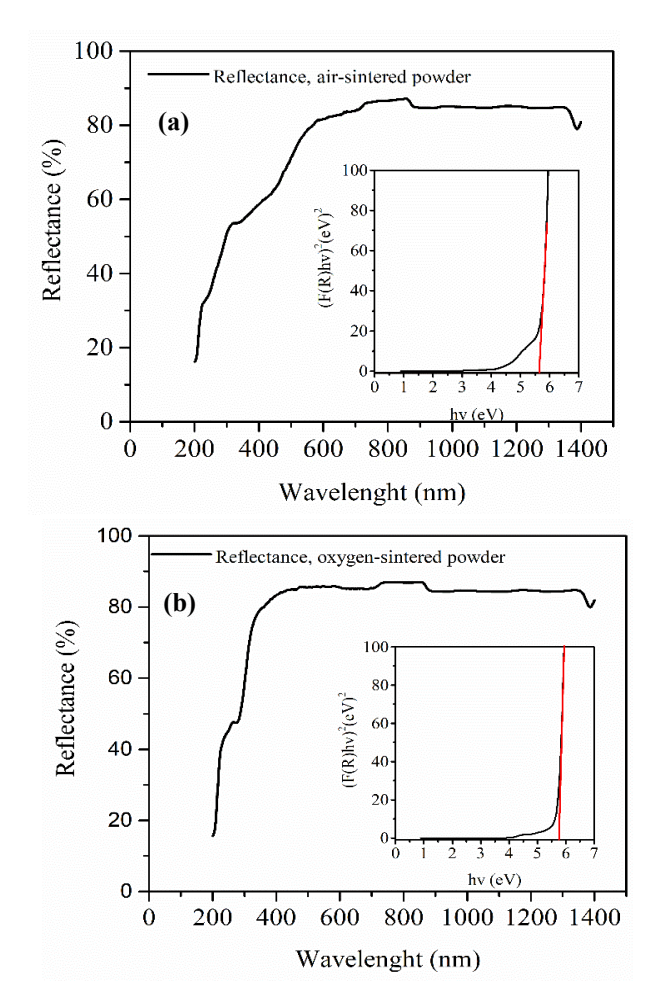


**Figure 6.** UV-Vis-NIR diffuse reflectance spectra of Ga-LLZO powder sintered in a) air and b) O<sub>2</sub>, the inner graphs were obtained using the reflectance data

by extrapolating the linear part of the  $[F(R)hv]^{\gamma}$  vs hv plot to the x-axis shown as an inner graph in Fig. 6 [43-44]. The indirect electronic band gap

**Table 4.** Comparison of bandgap energy values obtained with UV-Vis. absorption spectroscopy and UV-Vis. diffuse reflectance spectroscopy

		1 17	
		Indirect bandgap energy (eV)	Direct bandgap energy (eV)
Air-sintered powder	UV-Vis DRS. technique	5.64	5.18
	UV-Vis Abs. technique	5.42	4.63
Oxygen-sintered powder	UV-Vis DRS. technique	5.77	5
	UV-Vis Abs. technique	4.92	3.85

energy of the oxygen-sintered sample, Eg-<sub>02</sub>=5.77 eV, is relatively larger than that of the air-sintered sample, Eg-air=5.64 eV. The direct band gap also widens when the sample is sintered in oxygen (E<sub>g-O2</sub>=5.18 eV, E<sub>g-air</sub>=5 eV). The literature reports that point defects like oxygen vacancies narrow the band gap by inducing intraband gap energy states [45]. On the other hand, it is well-known that high temperatures, required for dense LLZO pellets, lead Li to evaporate by creating oxygen vacancies to preserve the charge neutrality of the lattice [46-47]. That's why we can say that low partial oxygen pressure in the air most likely increased the oxygen vacancy concentration and caused a band gap narrowing [48].

We have also obtained bandgap energies of the samples by using the UV-Vis. absorption spectroscopy to compare the results of UV-Vis. diffuse reflectance spectroscopy. LLZO powders were dispersed in a solvent for UV-Vis absorption measurements. As shown in Table 4., narrower bandgaps were obtained with the UV-Vis. absorption spectroscopy technique for both samples. Furthermore, while the obtained band gap energy of the oxygen-sintered sample is relatively larger than that of the air-sintered sample with the UV-Vis DRS technique, it is obtained narrower with the UV-Vis absorption technique. The difference is most probably due to the fact that LLZO powder is not soluble, and the dispersion of the powders is not stable. That's why scattering effects occur which are not taken into account by the UV-Vis absorption spectroscopy.

#### 4. Conclusion

In this work, we have studied the effects of sintering atmospheres on the optical, structural, and conductivity properties of Ga-doped LLZO solid electrolytes. Both samples sintered in oxygen and air showed a cubic crystal structure. The electronic indirect band gap energy of the oxygen-sintered sample was obtained relatively larger, E<sub>g</sub>=5.77 eV, compared to the air-sintered sample with UV-Vis DRS spectroscopy. SEM and 3D optical profilometer results indicated that the oxygen-sintered pellet was formed with lower porosity consequently leading to a higher relative density.

Furthermore, ionic conductivities also confirmed the density difference of the pellets. According to the EIS results, the oxygen-sintered pellet has a high ionic conductivity of  $1.04 \times 10^{-4} \, \mathrm{Scm^{-1}}$ . Also, the 3D optical profilometer measured a lower surface root-mean-square (RMS) roughness of  $Rq = 0.1833 \, \mu \mathrm{m}$  for the oxygen-sintered pellet which can be useful to create an intimate interface with Li anode to suppress the Li growth.

#### **Article Information Form**

#### **Funding**

The author has received financial support from Selçuk University of Priority Area Research Project with the number of 21406002 for the research, authorship or publication of this study.

## The Declaration of Conflict of Interest/ Common Interest

No conflict of interest or common interest has been declared by the authors.

The Declaration of Ethics Committee Approval
This study does not require ethics committee
permission or any special permission.

# The Declaration of Research and Publication Ethics

The author of the paper declare that they comply with the scientific, ethical and quotation rules of SAUJS in all processes of the paper and that they do not make any falsification on the data collected. In addition, they declare that Sakarya University Journal of Science and its editorial board have no responsibility for any ethical violations that may be encountered, and that this study has not been evaluated in any academic publication environment other than Sakarya University Journal of Science.

### Copyright Statement

The author owns the copyright of their work published in the journal and their work is published under the CC BY-NC 4.0 license.

#### References

- [1] A. Machín, C. Morant, F. Márquez, "Advancements and Challenges in Solid-State Battery Technology: An In-Depth Review of Solid Electrolytes and Anode Innovations," Batteries, vol. 10, no. 1, pp. 29, 2024.
- [2] W. Feng, Y. Zhao, Y. Xia, "Solid Interfaces for the Garnet Electrolytes," Advanced Materials, vol. 36, pp. 2306111, 2024.
- [3] F. Öksüzoğlu, Ş. Ateş, O. M. Özkendir, G. Çelik, Y. R. Eker, H. Baveghar, "Structure and ionic conductivity of NASICON-type LATP solid electrolyte synthesized by the solid-state method," Ceramics International, 2024.
- [4] S. Saran, Y. R. Eker, Ş. Ateş, G. Çelik, H. Baveghar, O. M. Özkendir, W. Klysubun, "The effect of Ti to the crystal structure of Li<sub>7-3x</sub>M<sub>x</sub>La<sub>3</sub>Zr<sub>1.8</sub>Ti<sub>0.2</sub>O<sub>12</sub> (M=Ga, In) garnet-type solid electrolytes as a second dopant," Advances in Applied Ceramics, vol. 121, pp. 238-246, 2022.
- [5] S. Saran, O. M. Özkendir, Ü. Atav, "The effect of two different substituted atoms in lithium positions on the structure of garnet-type solid electrolytes," Turkish Journal of Physics, vol. 45, no. 3, pp. 148-158, 2021.
- [6] Y. Li, Z. Cao, Z. Jiang, Y. Cao, J. Liu, L. Wang, "Synergistic effect of Ga and Yb co-

- doping on the structure and ionic conductivity of Li<sub>7</sub>La<sub>3</sub>Zr<sub>2</sub>O<sub>12</sub> ceramics," Ionics, vol. 28, pp. 5321-5331, 2022.
- [7] W. Xia, B. Xu, H. Duan, Y. Guo, H. Kang, Li, H. Liu, "Ionic conductivity and air stability of Al-doped Li<sub>7</sub>La<sub>3</sub>Zr<sub>2</sub>O<sub>12</sub> sintered in alumina and Pt crucibles," ACS applied materials & interfaces, vol.8, no. 8, pp. 5335-5342, 2016.
- [8] S. Saran, Y. R. Eker, "Synthesis, structural and conductive properties of Nd doped garnet-type Li<sub>7</sub>La<sub>3</sub>Zr<sub>2</sub>O<sub>12</sub> Li-ion conductor," Current Applied Physics, vol. 41, pp.1-6, 2022.
- [9] C. Li, Y. Qiu, Y. Zhao, W. Feng, "Self assembled electron blocking and lithiophilic interface towards dendrite-free solid-state lithium battery," Chinese Chemical Letters, vol. 35, no. 4, pp. 108846, 2024.
- [10] M. Philipp, B. Gadermaier, P. Posch, I. Hanzu, S. Ganschow, M. Meven, D. Rettenwander, G. J. Redhammer, H. M. R. Wilkening, "The Electronic Conductivity of Single Crystalline Ga-Stabilized Cubic Li<sub>7</sub>La<sub>3</sub>Zr<sub>2</sub>O<sub>12</sub>: A Technologically Relevant Parameter for All-Solid-State Batteries," Advanced Materials Interfaces, vol. 7, pp. 2000450, 2020.
- [11] K. Kerman, A. Luntz, V. Viswanathan, Y. M. Chiang, Z. B. Chen, "Review-practical challenges hindering the development of solid-state Li-ion batteries," Journal of Electrochemical Society, vol. 164, pp. A1731–A1744, 2017.
- [12] C. L. Tsai, V. Roddatis, C. V. Chandran, Q. Ma, S. Uhlenbruck, M. Bram, P. Heitjans, O. Guillon, "Li<sub>7</sub>La<sub>3</sub>Zr<sub>2</sub>O<sub>12</sub> interface modification for Li dendrite prevention," ACS Applied Materials Interfaces, vol. 8, pp. 10617-10626, 2016.
- [13] A. Sharafi, E. Kazyak, A. L. Davis, S. Yu,
   T. Thompson, D. J. Siegel, N. P. Dasgupta,
   J. Sakamoto, "Surface chemistry mechanism of ultra-low interfacial

- resistance in the solid-state electrolyte Li<sub>7</sub>La<sub>3</sub>Zr<sub>2</sub>O<sub>12</sub>," Chemistry of Materials, 29, 7961-7968, 2017.
- [14] F. Han, A. S. Westover, J. Yue, X. Fan, F. Wang, M. Chi, D. N. Leonard, N. J. Dudney, H. Wang, C. Wang, "High electronic conductivity as the origin of lithium dendrite formation within solid electrolytes, "Nature Energy, vol. 4, pp. 187-196, 2019.
- [15] C. Du, Z. Li, Z. Fang, X. Fang, X. Ji, Z. Zhao, D. Liu, R. Li, X. Xiang, H. Yang, "Constructing a three-dimensional continuous grain boundary with lithiumion conductivity and electron blocking property in LLZO to suppress lithium dendrites," Journal of Alloys and Compounds, vol. 1003, pp. 175769, 2024.
- [16] X. Xiang, Z. Fang, C. Du, Z. Zhao, J. Chen, Y. Zhang, Q. Shen, "Constructing electron-blocking grain boundaries in garnet to suppress lithium dendrite growth," Journal of Advanced Ceramics, vol. 13, no. 2, pp. 166-175, 2024.
- [17] C. Xu, Y. Xue, M. Zhang, N. Liao, "Atomic-level designed LLZO electrolyte for LTO electrode in all-solid-state batteries with superb interfacial properties," Surfaces and Interfaces, vol. 40, pp. 103128, 2023.
- [18] T. Thompson, S. Yu, L. Williams, R. D. Schmidt, R. Garcia-Mendez, J. Wolfenstine, J. Sakamoto, "Electrochemical window of the Li-ion solid electrolyte Li<sub>7</sub>La<sub>3</sub>Zr<sub>2</sub>O<sub>12</sub>," ACS Energy Letters, vol. 2, no. 2, pp. 462-468, 2017.
- [19] K. Ajith, P. C. Selvin, K. P. Abhilash, P. Sivaraj, B. Nalini, G. G. Soundarya, "A correlative study on electrochemical and optical properties of LLZO (Li<sub>7</sub>La<sub>3</sub>Zr<sub>2</sub>O<sub>12</sub>) garnet electrolyte," Materials Today: Proceedings, vol. 50, pp. 2836-2839, 2022.
- [20] A. Escobedo-Morales, I. I. Ruiz-López, M.D. Ruiz-Peralta, L. Tepech-Carrillo, M.

- Sánchez-Cantú, J. E. Moreno-Orea, "Automated method for the determination of the band gap energy of pure and mixed powder samples using diffuse reflectance spectroscopy," Heliyon, vol. 5, no. 4, 2019.
- [21] A. E. Morales, E. S. Mora, U. Pal, "Use of diffuse reflectance spectroscopy for optical characterization of un-supported nanostructures," Revista mexicana de física, vol. 53, no. 5, pp. 18-22, 2007.
- [22] H. Lü, X. Chen, Q. Sun, N. Zhao, X. Guo, "Uniform garnet nanoparticle dispersion in composite polymer electrolytes, "Acta Physico-Chimica Sinica, pp. 2305016, 2024.
- [23] T. Eickhoff, P. Grosse, W. Theiss, "Diffuse reflectance spectroscopy of powders," Vibrational spectroscopy, vol. 1, no. 2, pp. 229-233, 1990.
- [24] H. Ranjan Sahu, G. Ranga Rao, "Characterization of combustion synthesized zirconia powder by UV-vis, IR and other techniques," Bulletin of Materials Science, vol. 23, pp. 349-354, 2000.
- [25] E. O. Filatova, A. S. Konashuk, "Interpretation of the changing the band gap of Al<sub>2</sub>O<sub>3</sub> depending on its crystalline form: connection with different local symmetries," The Journal of Physical Chemistry C, vol. 119, no. 35, pp. 20755-20761, 2015.
- [26] S. Rezaee, H. Araghi, H. Noshad, Z. Zabihi, "Physical characteristics of fluorine-doped lithium oxide as advanced material for solid-electrolyte-interphase applications of lithium-air batteries," The European Physical Journal Plus, vol. 137, no. 1194, 2022.
- [27] L. Robben, R. Merzlyakova, P. Heitjans, T. M. Gesing, "Symmetry reduction due to gallium substitution in the garnet Li6.43(2) Ga0.52 (3) La2. 67 (4) Zr2O12," Acta Crystallographica Section E: Crystallographic Communications, vol. 72, no. 3, pp. 287-289, 2016.

- [28] Ç. Kaya, F. Bondino, E. Magnano, H. Gündoğmuş, I. Ulfat, W. Klysubun, O. M. Ozkendir, "Influence of Gallium Substitution on the Crystal and Electronic Properties of Li5Ca<sub>1-x</sub>Ga<sub>x</sub>La<sub>3</sub>Zr<sub>2</sub>O<sub>12</sub> Solid State Battery Electrolyte," Journal of Electron Spectroscopy and Related Phenomena, vol. 226, pp. 45-52, 2018.
- [29] M. Matsui, K. Takahashi, K. Sakamoto, Hirano, Y. Takeda, O. Yamamoto, N. Imanishi, "Phase stability of a garnet-type lithium ion conductor Li<sub>7</sub>La<sub>3</sub>Zr<sub>2</sub>O<sub>12</sub>," Dalton Transactions, vol. 43, no. 3, pp.1019-1024, 2024.
- [30] F. Shen, W. Guo, D. Zeng, Z. Sun, J. Gao, J. Li, X. Han, "A simple and highly efficient method toward high-density garnet-type LLZTO solid-state electrolyte," ACS applied materials & interfaces, vol. 12, no. 27, pp. 30313-30319, 2020.
- [31] Y. Li, Z. Wang, C. Li, Y. Cao, X. Guo, "Densification and ionic-conduction improvement of lithium garnet solid electrolytes by flowing oxygen sintering," Journal of Power sources, vol. 248, pp. 642-646, 2014.
- [32] B. P. Dubey, A. Sahoo, V. Thangadurai, Y. Sharma, "Morphological, dielectric and transport properties of garnet-type Li6.25+yAl0.25La3Zr2-yMnyO12 (y= 0, 0.05, 0.1, and 0.2)," Solid State Ionics, vol. 351, pp. 115339, 2020.
- [33] A. B. Gadkari, T. J. Shinde, P. N. Vasambekar, "Structural analysis of Sm<sup>3+</sup> doped nanocrystalline Mg-Cd ferrites prepared by oxalate co-precipitation method," Materials characterization, vol. 60, no. 11, pp. 1328-1333, 2009.
- [34] W. Feng, X. Dong, P. Li, Y. Wang, Y. Xia, "Interfacial modification of Li/Garnet electrolyte by a lithiophilic and breathing interlayer," Journal of Power Sources, vol. 419, pp. 91-98, 2019.

- [35] V. Raj, K. G. Naik, B. S. Vishnugopi, A. K. Rana, A. S. Manning, S. R. Mahapatra, D. Mitlin, "Dendrite Growth-Microstructure-Stress-Interrelations in Garnet Solid-State Electrolyte," Advanced Energy Materials, vol. 14, no. 15, pp. 2303062, 2024.
- [36] A. Baniya, A. Gurung, J. Pokharel, K. Chen, R. Pathak, B. S. Lamsal, Q. Qiao, "Mitigating interfacial mismatch between lithium metal and garnet-type solid electrolyte by depositing metal nitride lithiophilic interlayer," ACS Applied Energy Materials, vol. 5, no. 1, pp. 648-657, 2022.
- [37] J. Zhang, R. Yu, J. Li, H. Zhai, G. Tan, X. Tang, "Transformation of undesired Li<sub>2</sub>CO<sub>3</sub> into lithiophilic layer via double replacement reaction for garnet electrolyte engineering," Energy & Environmental Materials, vol. 5, no. 3, pp. 962-968, 2022.
- [38] H. Huo, Y. Chen, N. Zhao, X. Lin, J. Luo, X. Yang, X. Sun, "In-situ formed Li<sub>2</sub>CO<sub>3</sub>-free garnet/Li interface by rapid acid treatment for dendrite-free solid-state batteries," Nano Energy, vol. 61, pp. 119-125, 2019.
- [39] F. Du, T. Liao, T. Ye, Y. Wu, G. Guo, K. Zhu, Z. Xie, "Room-temperature, all-solid-state lithium metal batteries enabled by a moderate-temperature formation method," Journal of Materials Science, vol. 1, no. 10, 2022.
- [40] L. Wang, Y. Lu, C. Zheng, M. Cai, F. Xu, Z. Wen, "In Situ Construction of a Lithiophilic and Electronically Insulating Multifunctional Hybrid Layer Based on the Principle of Hydrolysis for a Stable Garnet/Li Interface," Advanced Functional Materials, pp. 2402971, 2024.
- [41] S. Gunaydin, H. Miyazaki, S. Saran, H. Baveghar, G. Celik, M. Harfouche, M. Abdellatief, O. M. Ozkendir, "The Effect of CrFe<sub>2</sub>O<sub>4</sub> Addition on the Ionic Conductivity Properties of Manganese-Substituted LiFeO<sub>2</sub> Material, "Journal of

Electronic Materials, vol. 53, pp. 367-379, 2024.

- [42] F. Öksüzoğlu, S. Ateş, O. M. Özkendir, G. Çelik, Y. R. Eker, H. Baveghar, M. A. Basyooni-M. Kabatas, "The Impact of Boron Compounds on the Structure and Ionic Conductivity of LATP Solid Electrolytes," Materials, vol. 17, pp. 3846, 2024.
- [43] S. Landi Jr, I. R. Segundo, E. Freitas, M. Vasilevskiy, J. Carneiro, C. J. Tavares, "Use and misuse of the Kubelka-Munk function to obtain the band gap energy from diffuse reflectance measurements," Solid state communications, vol. 341, pp. 114573, 2022.
- [44] P. Makuła, M. Pacia, W. Macyk, "How to correctly determine the band gap energy of modified semiconductor photocatalysts based on UV-Vis spectra," The journal of physical chemistry letters, vol. 9, no. 23, pp. 6814-6817, 2018.
- [45] A. Sarkar, C. Loho, L. Velasco, T. Thomas, S. S. Bhattacharya, H. Hahn, R. Djenadic, "Multicomponent equiatomic rare earth oxides with a narrow band gap and associated praseodymium multivalency," Dalton transactions, vol. 46, no. 36, pp. 12167-12176, 2017.
- [46] N. Kuganathan, M. J. Rushton, R. W. Grimes, J. A. Kilner, E. I. Gkanas, A. Chroneos, "Self-diffusion in garnet-type Li<sub>7</sub>La<sub>3</sub>Zr<sub>2</sub>O<sub>12</sub> solid electrolytes," Scientific Reports, vol. 11, no. 1, pp. 451, 2021.
- [47] Z. Ma, B. Zhao, W. Li, S. Jiao, W. Gong, H. Qiu, M. Yu, "Effects of fabrication atmosphere conditions on the physicochemical properties of garnet electrolyte," Ionics, vol. 28, no. 6, pp. 2673-2683, 2022.
- [48] X. Ping, Q. Zheng, B. Meng, W. Lin, Y. Chen, C. Fang, W. Liang, "Influence of sintering atmosphere on the phase, microstructure, and lithium-ion conductivity of the Al-doped Li<sub>7</sub>La<sub>3</sub>Zr<sub>2</sub>O<sub>12</sub>

solid electrolyte," Ceramics International, vol. 48, no. 18, pp. 25689-25695, 2022.